Report on the Fundamentals of Ab-initio Methods

Karel Stryczek

Advisor: Assoc. Prof. Antonio Cammarata, PhD,
Ing. Matuš Kaintz

Faculty of Electrical Engineering

Czech Technical University

Prague, Czech Republic

Date: July 8, 2025

This report is written to exhibit an understanding of the contents it discusses.

1 Introduction

The purpose of this report is to demonstrate an understanding of ab-initio methods and their implementation in the ABINIT software via Density Functional Theory calculations. Ab-initio refers to calculations from first physical principles that predict properties of materials without empirical observation. The report begins with a preliminary understanding of the physics behind these ab-initio calculations before moving to specific calculations of the band structure of silicon at various doping levels of carbon. The band structure is perhaps the most useful measure of a semi-conductor's use in electronic devices such as photovoltaics, transistors, and diodes. The band structure of semi-conductors can be intuitively defined as in between that of insulators and conductors, since they still have a band gap, though not high enough to be considered an insulator. This report considers the band structure of silicon at high carbon doping, essentially considering an 8 atom supercell of silicon that progressively has 1 silicon atom replaced by a carbon atom at each case, for 9 cases total.

2 Theory

2.1 Crystal Lattice and Primitive Cell

When crystal systems are considered, the *crystal lattice* is defined as a repeating arrangement of atoms or molecules that make up the crystalline solid [2]. Moreover, there is a basis or motif of atoms that is repeated infinitely in the lattice. This assumption is not always true, but we are only considering crystal systems here. We can begin to define the entire solid's crystal structure by defining three vectors: $\boldsymbol{a}$, $\boldsymbol{b}$, $\boldsymbol{c}$ that form a repeatable pattern and then take any linear combination of these vectors:

$$\boldsymbol{T} = u_1\boldsymbol{a} + u_2\boldsymbol{b} + u_3\boldsymbol{c}. \tag{1}$$

Where u_1, u_2, u_3 are integers. The space enclosed by these vectors is called the *unit cell*. The volume of the unit cell is defined in Equation 2.

$$V = |\boldsymbol{a} \cdot \boldsymbol{b} \times \boldsymbol{c}| \tag{2}$$

The unit cell of the smallest possible volume is called the *primitive unit cell*, where $\boldsymbol{a}$, $\boldsymbol{b}$, $\boldsymbol{c}$ would be considered the primitive lattice vectors, this is portrayed in Figure 1, a primitive cell of carbon, whose volume is defined with the black boundary lines. There is also the conventional unit cell, which is larger than the primitive unit cell, but makes clear the symmetries of the crystal structure. This can just as well be chosen as the primitive cell, so it is clear the primitive cell is not unique. Moreover, *lattice points* are points within the lattice that contain locations of atoms or molecules as they are repeated throughout the crystal structure. A common choice for primitive cell is the Wigner-Seitz cell, which is defined as the smallest area enclosed by bisecting lines connecting these lattice points.

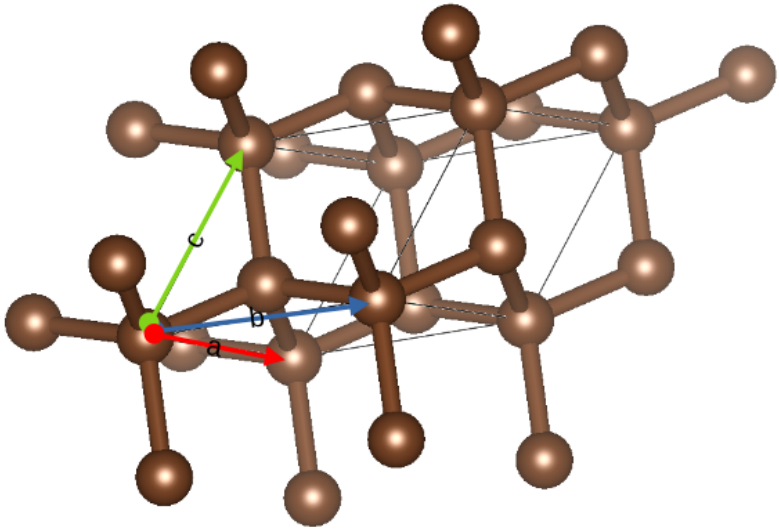

Figure 1: Primitive Cell of Carbon

Finally, we can classify 230 space groups that each have varying levels of possible symmetry, this includes rotation, translation, point symmetries, as well as many others. The 14 Bravais lattices are the conventional way of classifying different lattice types based on their geometry. [1, 2, 3]

2.2 Reciprocal Space

As mentioned in the prior section, the systems we deal with here are periodic, making the Fourier transform particularly useful, since just as the crystal is periodic, the properties of the solid will also be periodic. We define the Fourier transform of the lattice as:

$$g(\boldsymbol{r}) = \frac{1}{V}\int_V g(\boldsymbol{G})e^{i\boldsymbol{G}\cdot\boldsymbol{r}} \tag{3}$$

where V is the volume of the considered cell, $g(\boldsymbol{r})$ is the periodic function of the physical property that is invariant under translations, and $\boldsymbol{G}$ are vectors specifying the lattice points in reciprocal space as per:

$$\boldsymbol{G} = v_1\boldsymbol{a}^* + v_2\boldsymbol{b}^* + v_3\boldsymbol{c}^* \tag{4}$$

where v_1, v_2, v_3 are integers. We can define these reciprocal lattice vectors in the following equations:

$$\boldsymbol{a}^* = 2\pi\frac{\boldsymbol{b}\times\boldsymbol{c}}{|\boldsymbol{a}\cdot\boldsymbol{b}\times\boldsymbol{c}|}, \boldsymbol{b}^* = 2\pi\frac{\boldsymbol{c}\times\boldsymbol{a}}{|\boldsymbol{a}\cdot\boldsymbol{b}\times\boldsymbol{c}|}, \boldsymbol{c}^* = 2\pi\frac{\boldsymbol{a}\times\boldsymbol{b}}{|\boldsymbol{a}\cdot\boldsymbol{b}\times\boldsymbol{c}|}. \tag{5}$$

We can now define the Brillouin zone as the Wigner-Seitz cell in reciprocal space, as described in the previous section. Furthermore, the irreducible Brillouin zone (IBZ) can be defined as the smallest portion of the Brillouin zone that, through the crystal's symmetries, is sufficient to represent all physical properties. This is because the IBZ, through the symmetries of the crystal, can be used to reconstruct the entire Brillouin zone. [2, 3]

2.3 Time-Independent Schrodinger Equation

The key equation that we are solving in these calculations is the time independent Schrödinger equation [1]. This is because we take that observable quantities will not change in time, but only in space, this reduces the problem to a Hamiltonian eigenvalue problem as described in Equation 7.

$$H(\boldsymbol{r}) = -\frac{\hbar^2}{2m}\nabla^2 + V(\boldsymbol{r}) \tag{6}$$

$$H(\boldsymbol{r})\psi(\boldsymbol{r}) = E\psi(\boldsymbol{r}) \tag{7}$$

$H(\boldsymbol{r})$ is the Hamiltonian operator that represents the kinetic and potential energy of the system as defined in Equation 6, $\boldsymbol{r}$ is the position in Cartesian coordinates, E is the set of eigenvalues, and $\psi(\boldsymbol{r})$ are the eigenfunctions of the Hamiltonian operator. These wavefunctions also contain information about the quantum states of the particles in the system. [1, 3]

2.3.1 Bloch's Theorem

According to Bloch's theorem, the solutions to the Schrödinger equation in a periodic potential can be expressed in the form:

$$\psi(\boldsymbol{r}) = u(\boldsymbol{r})e^{i\boldsymbol{k}\cdot\boldsymbol{r}}. \tag{8}$$

Where $\boldsymbol{r}$ is Cartesian position, u is a periodic function with the same periodicity as the lattice, ψ is the wavefunction, and $\boldsymbol{k}$ is a reciprocal lattice vector. This will become important in the next section. [1]

2.3.2 Periodic Potential Schrödinger Equation

The Schrödinger Equation can be rewritten for the case of a periodic potential, as would be seen in a crystal lattice. We can use Bloch's theorem and Equation 6 to find the Schrödinger Equation for a system with a periodic potential, which will allow us to solve for eigenvalues of the Hamiltonian at individual $\boldsymbol{k}$ points in the Brillouin zone:

$$H(\boldsymbol{r})u_{i,\boldsymbol{k}}(\boldsymbol{r})e^{i\boldsymbol{k}\cdot\boldsymbol{r}} = E_{i,\boldsymbol{k}}u_{i,\boldsymbol{k}}(\boldsymbol{r})e^{i\boldsymbol{k}\cdot\boldsymbol{r}} \tag{9}$$

$$e^{i\boldsymbol{k}\cdot\boldsymbol{r}}H(\boldsymbol{r})e^{-i\boldsymbol{k}\cdot\boldsymbol{r}}u_{i,\boldsymbol{k}}(\boldsymbol{r}) = E_{i,\boldsymbol{k}}u_{i,\boldsymbol{k}}(\boldsymbol{r}) \tag{10}$$

$$H(\boldsymbol{r},\boldsymbol{k})u_{i,\boldsymbol{k}}(\boldsymbol{r}) = E_{i,\boldsymbol{k}}u_{i,\boldsymbol{k}}(\boldsymbol{r}) \tag{11}$$

$$H(\boldsymbol{r},\boldsymbol{k}) = -\frac{\hbar}{2m}(\nabla + i\boldsymbol{k})^2 + V(\boldsymbol{r}). \tag{12}$$

This final form of the one particle Hamiltonian, derived from Equation 6, is specifically suited for solving problems involving periodic potentials and allows us to compute eigenvalues of the Hamiltonian at individual $\boldsymbol{k}$ points in the Brillouin zone. Although the eigenvalues of such systems are discrete, the number of atoms in a typical solid is on the order of 10^{23} or more. Each atom has its own discrete energy levels, and due to the overlap of atomic orbitals in the crystal, these discrete levels broaden into continuous energy bands. This phenomenon gives rise to the concept of *band structure*, continuous bands of energy that can be occupied by electrons in a crystalline solid. [1]

In band structure calculations, we take the IBZ and define it using a set of $\boldsymbol{k}$ points that define a piecewise linear path in reciprocal space. We then compute the energy levels available at each of these points and plot these energies against the high symmetry $\boldsymbol{k}$ points to get our band structure. This significantly reduces the computational cost by taking advantage of the symmetries present in the IBZ and is a common method of computing band structure. This is because the IBZ is defined as the smallest portion of the Brillouin zone that can still be used to reconstruct the full Brillouin zone through the crystal's symmetries. Recall that in theory, there are an infinite amount of the $\boldsymbol{k}$ points, so it is impossible to compute them all, thus it is important to consider the amount of $\boldsymbol{k}$ points and in what manner they are distributed to get the accurate results, and the high symmetry path is the best way to do this when considering band structure calculations. [1, 3, 4]

2.4 Density Functional Theory (DFT)

2.4.1 Motivating Problem

As mentioned, we wish to solve the eigenvalue problem for the Hamiltonian and its eigenfunctions. The problem now is that, since we are considering a solid comprised of many particles, we must solve the many body Schrödinger equation. This is problematic as the equation is intractable if we do not make any approximations. However, this is where the benefit of DFT shines, as we can take our many body problem and reduce it to the computation of the electron density $\rho(\boldsymbol{r})$.

2.4.2 Hohenberg-Kohn Theorems

In summary of the two theorems that lay the basis for DFT, the ground state energy E is a unique functional of the electron charge density (ρ) and can be written $E[\rho]$. In principle, this electron charge density is the key to computing all aspects of the material under study. [3]

2.4.3 Kohn-Sham Equations

The Kohn-Sham Equations where introduced in 1965 in the paper titled "Self-Consistent Equations Including Exchange and Correlation Effects" by Kohn and Sham [5]. These equations yield the one electron orbitals, called Kohn-Sham orbitals ϕ that comprise the electron density in the following relationship:

$$\rho(\boldsymbol{r}) = \sum_{i=1}^{N} |\phi_i(\boldsymbol{r})|^2 \tag{13}$$

Kohn and Sham also show that the exact ground-state energy of an n electron system can be written as:

$$E[\rho] = \frac{-\hbar^2}{2me} \sum_{i=1}^{n} \int \phi_i^*(\boldsymbol{r_1}) \nabla^2 \phi_i(\boldsymbol{r_1}) d\boldsymbol{r_1} - j_0 \sum_{I=1}^{N} \frac{Z_I}{r_I} \rho(\boldsymbol{r_1}) d\boldsymbol{r_1} + \frac{1}{2} j_0 \int \int \frac{\rho(\boldsymbol{r_1})\rho(\boldsymbol{r_2})}{r_{12}} d\boldsymbol{r_1} d\boldsymbol{r_2} + E_{XC}(\rho) \tag{14}$$

$$j_0 = \frac{e^2}{4\pi\epsilon_0}. \tag{15}$$

This energy functional is made up of four terms: the kinetic energy of electrons, the attractive Coulomb potential between nuclei and electrons, the electrostatic repulsion potential between electrons and electrons, and exchange correlation energy. We now move on to the Kohn-Sham equations which are used to compute the Kohn-Sham orbitals. The Kohn-Sham equations are of the form:

$$\left\{ -\frac{\hbar^2}{2m_e} \nabla_1^2 - j_0 \sum_{I=1}^{N} \frac{Z_I}{r_{I1}} + j_0 \int \frac{\rho(\boldsymbol{r}_2)}{r_{12}} d\boldsymbol{r_2} + V_{XC}(\boldsymbol{r_1}) \right\} \phi_i(\boldsymbol{r_1}) = E_i \phi_i(\boldsymbol{r_1}). \tag{16}$$

With the term V_{XC}, the exchange-correlation potential defined as the functional derivative of the electron charge density:

$$V_{XC}[\rho] = \frac{\delta E_{XC}[\rho]}{\delta \rho}. \tag{17}$$

The calculation of the converged charge density using the self-consistent field method (SCF) is as follows:

1. Guess of an initial $\rho(\boldsymbol{r})$
2. Use the initial ρ and E_{XC} to compute the exchange correlation potential V_{XC} (Equation 17)
3. Calculate Kohn-Sham orbitals (Equation 16)
4. Update the charge density (Equation 13)

5. Calculate the total energy (Equation 14)

6. Repeat these steps until reaching some predefined convergence bound on difference of total energies between updated densities i.e until self-consistency is reached

In most cases, the Kohn-Sham orbitals are expressed using a linear combination of basis functions. The coefficients of this linear expansion are then of interest, and can be solved for using matrix manipulation. This set of basis functions is discussed in further detail as a part of the consideration of convergence criteria regarding the cutoff energy. [1, 3, 5]

2.4.4 Pseudopetentials

Pseudopotentials are an approximation technique employed in DFT calculations. The use of pseudopotentials takes advantage of the fact that core electrons, closer to the nucleus, do not take part in bonding, though they would add some computational cost to account for in practice. Pseudopotentials get rid of the need to account for these electron and nucleus interactions and replace them with one effective potential. This speeds up computation and removes the need to account for these unnecessary particles. For these reasons, they are implemented almost always in practice as either Norm-conserving pseudopotentials or Projector Augmented Wave pseudopotentials (PAW). [3]

2.4.5 Exchange Correlation Functionals

The exchange correlation functional is part of the computation scheme described in subsubsection 2.4.3. The closed form of this E_{XC} term is unknown, though approximations exist. These approximations are conitnuously being created and are an active part of DFT research. [3]

The Localized Density Approximation (LDA) is the simplest and earliest form of this exchange correlation functional [3]. The key assumption made in LDA is that the electron density varies slowly in space. Thus, LDA is best used in systems with relatively uniform electron densities.

The Generalized Gradient Approximation (GGA) incorporates the gradient of the density function. This is the form we consider in our computations as per the PBE-GGA functional. [3]

2.5 Electronic Structure

This section is meant to describe fundamental ideas that will be expanded upon in the further sections regarding Band Structure.

2.5.1 Fermi-Dirac Distribution

The Fermi-Dirac distribution is fundamental to understanding the probability of an electron occupying a given energy state and is described by Equation 18. The *Fermi level* is the point in the distribution where there is exactly a 50% chance of occupation.

$$p(E) = \frac{1}{1 + e^{\frac{E - E_F}{k_B T}}} \tag{18}$$

Where we can see if $E = E_F$, or in other words, the energy is equal to the Fermi level, we have a 50% chance of occupancy, regardless of temperature, k_B is the Boltzmann constant, and T is temperature. It is worth noting that when the Fermi level is defined for insulators or semiconductors, it lies where there are actually no occupied states, within a gap that is defined in the next section. [3]

2.5.2 Valence and Conduction Bands

The valence band consists of the possible energy levels of the valence or outermost electrons, those that participate in bonding. The conduction band is made up of energy levels of electrons able to freely move throughout the material, these contribute to the conductivity. There may be gaps between any of these bands, or in other words, regions where there are no states able to be occupied. However, band gap typically refers to the gap between the valence band maximum and conduction band minimum, and is the same as observing the required energy for an electron to be promoted from the valence band to the conduction band, this energy is defined in the following equation:

$$E_{gap} = E_{CBM} - E_{VBM}. \tag{19}$$

If these minimum and maximum occur at the same $\boldsymbol{k}$ point, the band gap is classified as direct and promotion can be achieved with something as simple as shining a light onto the material whose frequency corresponds to the proper energy of promotion. If these occur at different $\boldsymbol{k}$ points, the gap is classified as indirect and electron promotion requires a phonon, a quantized vibration in the lattice, in combination with an added energy source, such as the aformetioned light source, making promotion less probable. Finally, the position of the Fermi level is a defining feature of the character of the material when it comes to electronic structure. Conductors will have their Fermi level crossing over states in the conduction band, while insulators and semiconductors will have the Fermi level placed within their band gap. [2, 3]

2.5.3 Density of States (DOS)

Density of states is a method in which we can observe at what exact energy there are available states for an electron to occupy. This is done by plotting the number of available states against specific energy values. Total DOS is computed with the following equation:

$$D(E) = \sum_{n,\boldsymbol{k}} w_{\boldsymbol{k}} \delta(E - E_{n,\boldsymbol{k}}) \tag{20}$$

where $D(E)$ is the states per energy, $w_{\boldsymbol{k}}$ is the weight of the $\boldsymbol{k}$ point, δ is the delta function, $E_{n,\boldsymbol{k}}$ is the eigenenergy for a particular band n at $\boldsymbol{k}$, and E is the energy in which we wish to analyze the amount of available states. The number of bands is also of interest, typically set to a considerably high number compared to the amount of required bands in order to capture unoccupied states. With respect to a material's classification, a conductor, or metallic material, will have available states in the conduction band. [3]

To analyze specific contributions from different orbitals onto the band structure we can take projected density of states (PDOS). In this case, we take the wave functions and project them onto Hydrogen-like orbitals akin to spherical harmonics. PDOS is particularly helpful in inspecting the contribution of doping atoms or defects, as it isolates contributions by atom and by orbital. Such a projection is described in the following equation: [3]

$$g(E) = \frac{1}{N_k} \sum_{n,\boldsymbol{k}} |\, \langle \phi | \psi_{n,\boldsymbol{k}} \rangle \,|^2 \delta(E_{n,\boldsymbol{k}} - E) \tag{21}$$

where ϕ are the Hydrogen-like orbitals defined with their associated quantum numbers, $\psi_{n,\boldsymbol{k}}$ are the Bloch functions, $E_{n,\boldsymbol{k}}$ is the energy corresponding to the Bloch function $\psi_{n,\boldsymbol{k}}$, and the term $\langle \phi | \psi_{n,\boldsymbol{k}} \rangle$ is associated with the project of the wave functions onto the hydrogen like orbitals, the magnitude of this quantity is then taken.

3 Computational Setup

3.1 Introduction

During these calculations, I employ the ABINIT software package. It has convenient use in Linux environments and uses DFT to compute a number of possible physical properties. The process for computing charge density as it is implemented in ABINIT is the same as that which is discussed in subsubsection 2.4.3.

3.1.1 An Overview of the Workflow

We first computed a converged $\boldsymbol{k}$ point scheme and plane wave basis set for the 2 atom primitive cell and used these converged values for the final computations using the 8 atom cell, this process is described in greater detail in the coming sections. In practice, there should be a convergence study done for the 8 atom cell, but the 2 atom cell values are deemed usable for the purposes of this report. Then, using these converged values, one must complete geometric optimization, this process is described in more detail later, but it is pertinent to gaining accurate values for use in band structure calculations. Finally, we can compute the band structure by computing eigenenergies at each $\boldsymbol{k}$ point using the converged charge densities from the SCF cycle. This calculation for band structure is done using a non-self consistent cycle (NSCF) with the charge density taken from the converged SCF, since we do not want to change the charge density, we select pre-determined high symmetry $\boldsymbol{k}$ points to compute these eigenergies

at. The high symmetry $\boldsymbol{k}$ points form a path that makes up the IBZ, the intervals between these points also sampled. This yields our final output, a plot of energy levels available at each $\boldsymbol{k}$ point. We also compute DOS and PDOS as part of the same input. Finally, we take Projector Augmented Wave pseudopotentials and run a fat bands calculation with the already converged density, which is another way of seeing PDOS.

3.2 Atomic Structure and Input Parameters

We first must define our supercell for use as an input. We begin with a 2 atom primitive cell of silicon and replicate it in a $2 \times 2 \times 1$ scheme within the VESTA software, this creates an 8 atom supercell that we then use for further calculation. Using phonopy is also an easy way to obtain the POSCAR file wherein the primitive vectors and positions of the 8 atoms within the cell are defined. Silicon is usually a Face-centered cubic material, however in our case, since we consider a supercell, it is really one face-centered orthorhombic. Moreover, we used Norm-conserving pseudoptentials for all computation except fat bands, where PAW pseudopotentials are used. Furthermore, the 8 atom supercell of silicon can be seen within the black boundaries in Figure 2. As a final note, ABINIT, by default, will check to see if the inputted parameters are a primitive cell, since we want to compute values for our supercell, we disable this feature, forcing ABINIT to consider the supercell as it is defined in input.

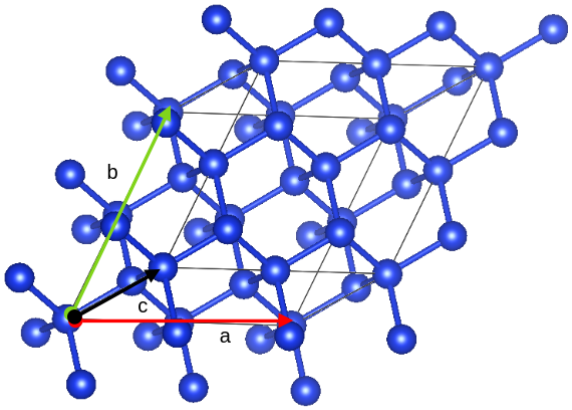

Figure 2: Supercell of Silicon

3.3 Convergence of Cutoff Energy and K Points

To make sure our calculations fall within reasonable values, we must first run convergence studies on both cutoff energy and $\boldsymbol{k}$ point mesh size. We do this by applying a double loop of cutoff energy and $\boldsymbol{k}$ point quantity; cutoff energy ranges from 20-65 Ha and $\boldsymbol{k}$ point mesh size ranges from $9 \times 9 \times 9$ to $23 \times 23 \times 23$ ($\boldsymbol{k}$ values were computed for the primitive cell and scaled to the supercell). We settled on values of 20 Ha and a

$\boldsymbol{k}$ point mesh of size $5 \times 5 \times 11$. These values are lower than what was used for 2 atom primitive cell preliminary calculations, but it makes sense to reduce the $\boldsymbol{k}$ mesh if we consider now a supercell, since the BZ is now actually smaller in reciprocal space.

3.3.1 Plane Waves

The cutoff energy is central to the amount and type of the plane wave basis set we use in calculation. In principle, there is an infinite amount of plane waves, so we must truncate it to some degree. We can do this by first considering our Bloch functions solutions ($\psi_{\boldsymbol{k}}(\boldsymbol{r}) = u_{\boldsymbol{k}}(\boldsymbol{r})e^{i\boldsymbol{k}\cdot\boldsymbol{r}}$) to the Schrödinger equation:

$$u_{\boldsymbol{k}}(\boldsymbol{r}) = \sum_{\boldsymbol{G}} c_{\boldsymbol{k}}(\boldsymbol{G})e^{i\boldsymbol{G}\cdot\boldsymbol{r}} \tag{22}$$

$$\psi_{\boldsymbol{k}}(\boldsymbol{r}) = \sum_{\boldsymbol{G}} c_{\boldsymbol{k}}(\boldsymbol{G})e^{i(\boldsymbol{G}+\boldsymbol{k})\cdot\boldsymbol{r}}. \tag{23}$$

The plane waves we consider are those with kinetic energy less than or equal to the cutoff energy defined as:

$$\frac{\hbar^2}{2m}|\boldsymbol{k}+\boldsymbol{G}|^2 \leq E_{cut}. \tag{24}$$

This is why we must check the convergence of the cutoff energy, since too little plane waves will yield poor results, but too many will do little to improve results but will increase the computational cost significantly. [3, 1]

3.4 Geometric Optimization

The key to geometric optimization is the Hellmann-Feynman Theorem which relates the derivative of the total energy with respect to a parameter to the expectation value of the derivative of the Hamiltonian with respect to that same parameter as shown in Equation 25.

$$\frac{dE}{d\lambda} = \langle\psi_\lambda|\frac{dH}{d\lambda}|\psi_\lambda\rangle \tag{25}$$

In the case of geometric optimization we wish to minimize the forces between atoms to ensure they are at rest. So, we want to iteratively sample these forces and then move the atoms accordingly to make certain there is no internal strain. From classical mechanics, the force is defined as the negative gradient of the energy, so we can rewrite the theorem as:

$$F = -\nabla_{\boldsymbol{r}}E = -\langle\psi(\boldsymbol{r})|\frac{dH}{d\boldsymbol{r}}|\psi(\boldsymbol{r})\rangle\,. \tag{26}$$

Here we have derived the method in which software such as ABINIT will compute these forces and then use any number of algorithms to move these atoms in the primitive cell accordingly to ensure a resting state of the system, which we then use for band structure calculations. It is also worthwhile to note that the Hellmann-Feynman theorem assumes a complete plane wave basis set, however, as we have noted before, this would be an infinite amount of functions and since we determine the amount and type of basis functions using the cutoff energy, a corrective term is typically added in geometric optimization to account for the incomplete basis function set. [1]

In our calculations we have set the convergence parameter for forces to 10^{-11}, aswell as allowing a shifting of both the cell volume and the primitive vectors. In Figure 3 we can observe the changing magnitude of the primitive vectors at each of the different dopant levels of carbon, beginning at pure silicon and ending up at pure diamond carbon. Vectors $\boldsymbol{a}$ and $\boldsymbol{b}$ were the ones replicated in the initial setup, so their magnitudes are generally the same. This graph is to be expected as the atomic radius of carbon is smaller than that of silicon. [1, 3]

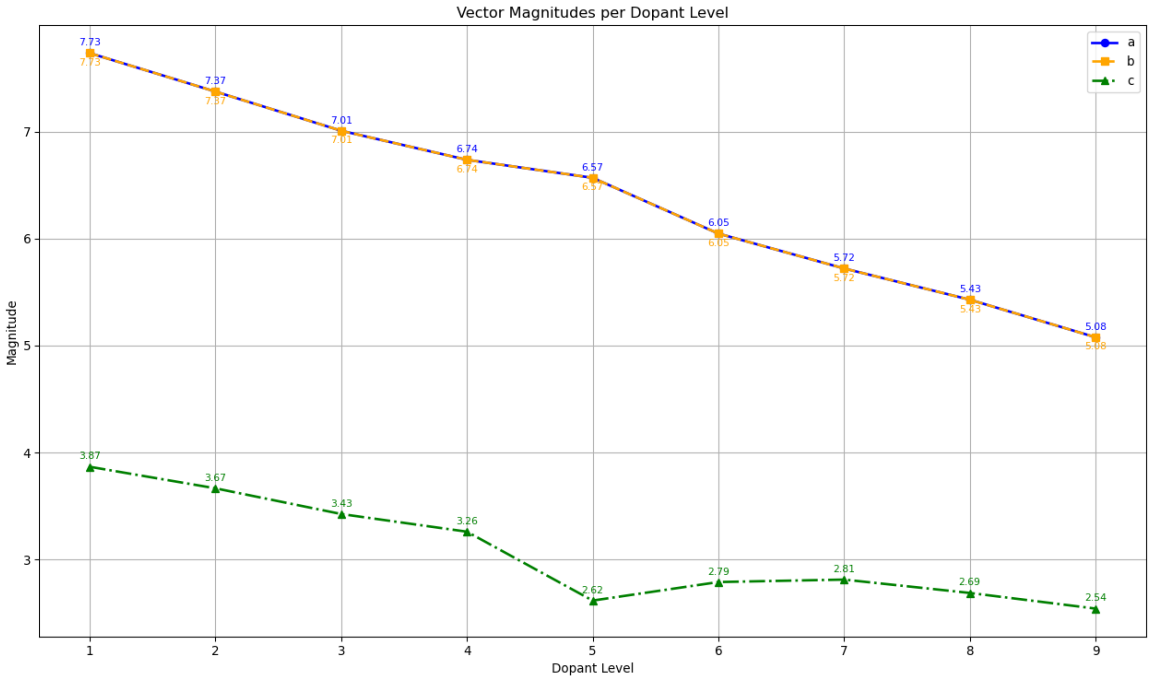

Figure 3: Plot of $\boldsymbol{a}$, $\boldsymbol{b}$, $\boldsymbol{c}$ Magnitudes Against different Dopant Levels

3.5 Band Structure Calculation

As alluded to earlier, we first define a high symmetry path of $\boldsymbol{k}$ points in the Brillouin zone and then define there to be divisions between each of these points on the path. We then perform a NSCF calculation that computes the eigenenergies at each of the $\boldsymbol{k}$ points that is then plotted on a Energy vs. $\boldsymbol{k}$ point graph. We actually receive two of these, one from the Monkhorst-Pack scheme and one from this high symmetry path. A notable fault of DFT calculations is that of underreporting the band gap, this is

rectified in a couple ways, namely GW calculations or Hybrid pseudopotentials, but for the purposes of this report we use Norm-conserving pseudopotentials and simply compare the changing structure at different dopant levels.[1]

3.6 Density of States Calculation

Finally, we also compute our DOS and PDOS, these are also computed using the NSCF cycle, but the wave functions taken from the SCF have some residual vector that must be converged when solving the eigenvalue problem, such a value is described in Equation 27.

$$r = ||H\psi - E\psi|| \tag{27}$$

This equation makes sure that the norm of the residual r is well converged to make sure the eigenvalues are accurate to a high order. Recall that this does not change the charge density, but is only recomputing these wave functions.

We then use Equation 20 to compute the number of states at each energy and then plot this number against the different energies. The DOS plots are essentially just histograms of number of states on the y axis and energy values on the x axis.

In our calculations we set the number of bands to 30 and the tolerance of wave function residuals to 10^{-22} to ensure well convergence when considering eigenvalues of the Hamiltonian. We then use these eigenenergies to compute total DOS and then project these wave functions on to the Hydrogen like orbitals as mentioned in subsubsection 2.5.3 These projected DOS are then plotted in the same way described earlier and allows observation of individual orbital contributions.[1, 3]

4 Output and Results

4.1 Band Structure

The band structure as computed for each dopant level, from 0% to 100% in increments of 12.5%, is reported here in Figure 4 using the high symmetry path. Each subfigure of Figure 4 is labeled with the number of silicon and carbon atoms are contained in the primitive cell.

We can conclude from Figure 4 that graphs b-e have no band gap and all others do, or in other words, b-e exhibit metallic type conductivity while all others are either insulators or semiconductors. The overlapping lowest unoccupied band and highest occupied band is the most clear way to see this, since it essentially means that electrons are free to jump to these conduction bands and move freely through the material. This is not exactly in line with other research, particularly the fact that e and f exhibit no band gap, however this may be attributed to our atomic structure in the supercell, since there are cluster defects introduced that are a result of not using the conventional cell.

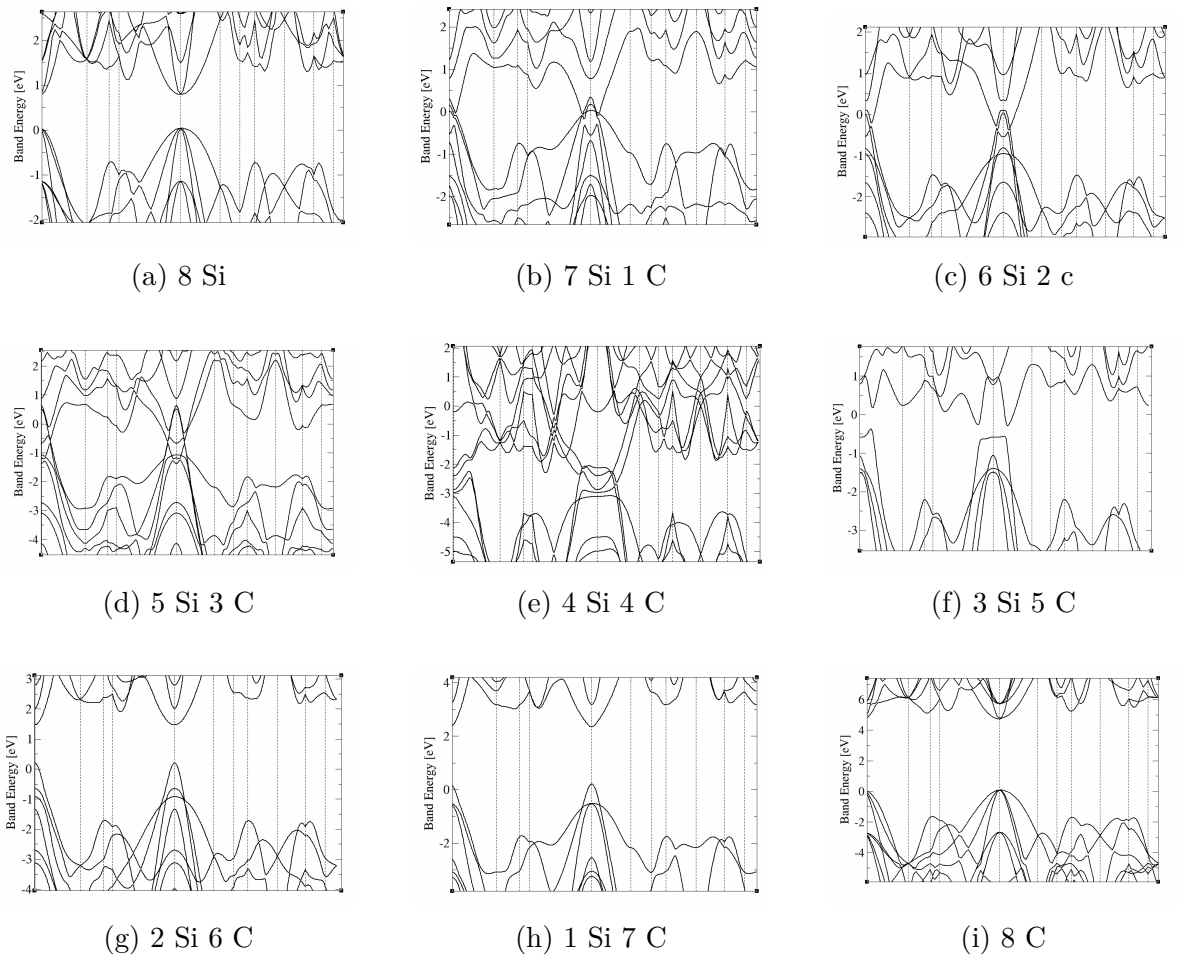

(a) 8 Si (b) 7 Si 1 C (c) 6 Si 2 c

(d) 5 Si 3 C (e) 4 Si 4 C (f) 3 Si 5 C

(g) 2 Si 6 C (h) 1 Si 7 C (i) 8 C

Figure 4: Band Structure of all 9 Dopant Levels

4.2 Total Density of States

The density of states is another method to assess the physical properties of the material, such as band gap. This is done by plotting the number of available states against their energies. Figure 5 displays the total DOS in the same manner as Figure 4.

The subfigures of Figure 5 are normalized in order for the Fermi level to be at 0, then states are plotted on states vs. energy axes. On plots such as Figure 5a and Figure 5i, the band gap is obvious, the area around 0 energy that has no available states. However, the drawback here is we cannot observe direct vs. indirect since there is no relationship here to $\boldsymbol{k}$ vectors.

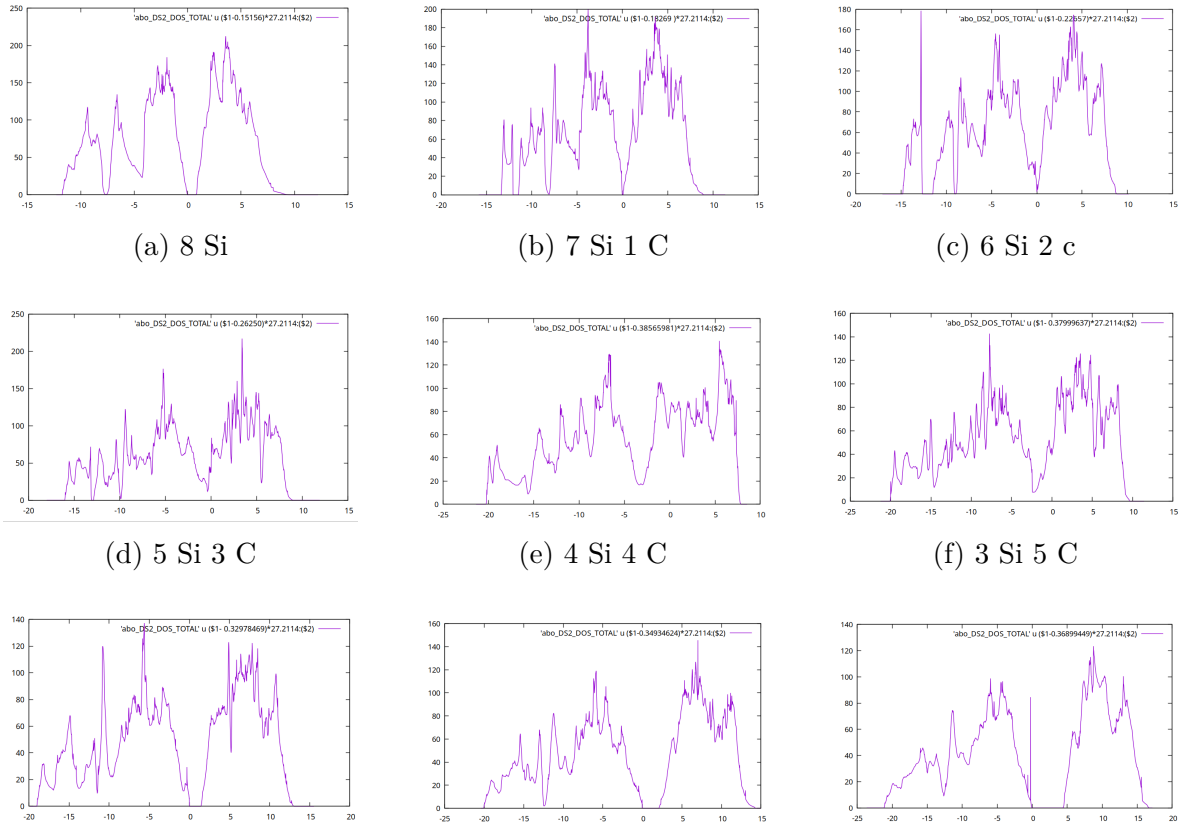

(a) 8 Si (b) 7 Si 1 C (c) 6 Si 2 c

(d) 5 Si 3 C (e) 4 Si 4 C (f) 3 Si 5 C

(g) 2 Si 6 C (h) 1 Si 7 C (i) 8 C

Figure 5: Overview of all 9 dopant levels

4.3 Band Gap

Band Gap was also calculated using the high symmetry path. If there was a band gap, its value is recorded in Table 1, these values are off from experimental values, though as mentioned before, this is to be expected. Recall, this is the energy difference between the highest occupied orbital in the valence band and the lowest unoccupied orbital in the conduction band.

Supercell	***k* path BG (eV)**
a	0.7819
f	0.08
g	1.2565
h	2.1305
i	4.6302

Table 1: Table of Calculated Band Gaps Pertaining to Figure 4 Band Structures

4.4 Projected Density of States and Fat Bands

4.4.1 Example of Interpretation of PDOS and Fat Bands

Density of states, especially the projected density of states allows us to analyze where electrons of individual atoms are contributing in the band structure, let us first compare fat bands and projected density of states to see that these are two different ways of seeing the same thing.

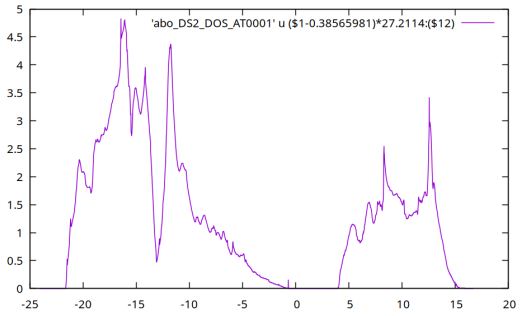

(a) PDOS of C1 in Diamond $l = 0$, $m_l = 0$

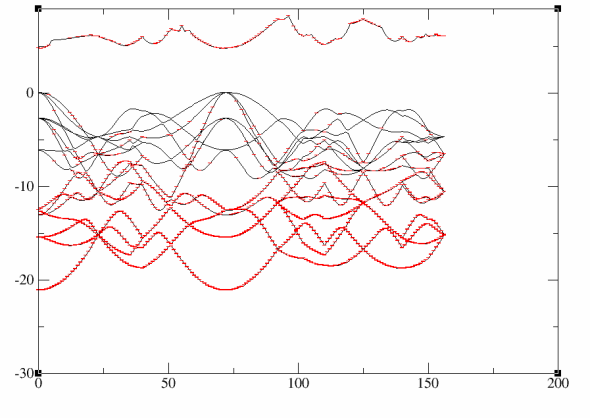

(b) Fat Bands of C1 in Diamond $l = 0$, $m_l = 0$

Figure 6: Projected Density of States and Fat Bands for C1 in Diamond

We can see that the more red areas of the fat bands plot in Figure 6 correspond to more contribution from that orbital, whereas the PDOS plot also shows this but by plotting the number of states this orbitals contributes. In this example case, we can see that in both plots the carbon atom in this position in the primitive cell, with quantum numbers $l = 0$ and $m_l = 0$ contributes mostly to energy levels between -20 and -10 eV, with lesser contributions to the conduction bands above the band gap.

4.4.2 Contribution of Dopant Orbitals in Reducing Band Gap

With the above example on how to interpret the graphs, we can discover which orbitals contribute to a reduced band gap. With what we learned in sections subsection 4.1-subsection 4.2, we can see that pure silicon has a band gap, however, 12.5% doping of carbon removes this gap, we should expect there to be states in the band gap contributed by this carbon atom.

The fat bands plot of this specific carbon orbital ($l = 0, m_l = 0$) points to heavy contributions deep in the valence bands, but more notably, there is great contribution of states at the bottom of the conduction band that are overlapping with the valence band, this is what was expected since the band gap disappeared after introducing the dopant carbon atoms.

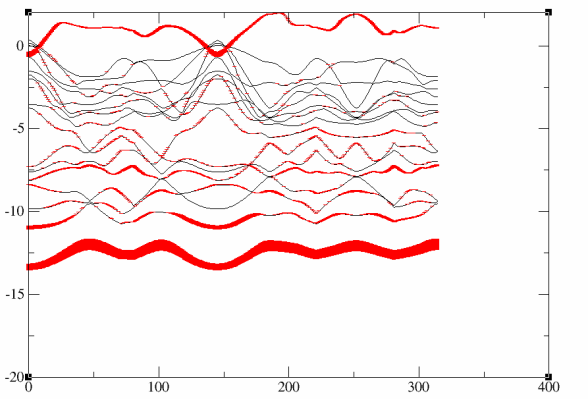

Figure 7: Fat Bands Plot for 12.5% C Doped Si with C Orbital $l = 0, m_l = 0$

5 Conclusion

5.1 Band Structure

We can see that introducing a dopant can severely change the band structure and even the class of material, as well as understand that this is fundamentally due to state contributed by a dopant. This change can be to the size of the gap or even the character of gap, direct or indirect. The doping level discussed is comparatively high compared to what is usually considered in practice, however this makes the changing band structure very apparent. Doping semiconductors is nothing novel, yet this is just another case study of how doping is an effective method of engineering band structure and band gap.

5.2 Errors and Scope of Enhancement

Converging to higher number of $\boldsymbol{k}$ points as well as higher cut off energy is perhaps the most obvious way to improve results, but this is entirely dependent on the magnitude of precision that is intended to achieve. A more severe way of decreasing error is that of switching pseudopotentials to hybrid methods, or using GW calculations. However, these are both more computationally expensive, and this is a common theme, the only way to fundamentally decrease the error here is to use more computationally expensive methods.

References

[1] P. W. Atkins and R. S. Friedman, *Molecular Quantum Mechanics*, Oxford University Press, 1996.
ISBN: 978-0-198-55948-1

[2] Charles Kittel, *Introduction to Solid State Physics*, Wiley IPL, 2004.
ISBN: 978-0-471-41526-8

[3] Matuš Kaintz, *Engineering Defect Clustering in Diamond-based Materials for Energy Harvesting and Other Technological Applications via Quantum-mechanical Descriptors*, PhD Dissertation Progress Report, Czech Technical University (CTU), 2025.

[4] H. J. Monkhorst and J. D. Pack, *Special points for Brillouin-zone integrations*, Phys. Rev. B, **13** (12), 5188–5192, 1976.
doi:10.1103/PhysRevB.13.5188

[5] W. Kohn and L. J. Sham, *Self-Consistent Equations Including Exchange and Correlation Effects*, Phys. Rev., **140** (4A), A1133–A1138, 1965.
doi:10.1103/PhysRev.140.A1133